

Manuscript Number: MARSYS-D-15-00297R1

Title: The relative roles of Modified Circumpolar Deep Water and sediment resuspension in maintaining the phytoplankton blooms above Pennell and Mawson Bank, Ross Sea.

Article Type: SI: Ross Sea

Keywords: iron; Manganese; Banks; Ross Sea; Modified Circumpolar Deep Water; Water mixing

Corresponding Author: Dr. Mariko Hatta, Sc.D

Corresponding Author's Institution:

First Author: Mariko Hatta, Sc.D

Order of Authors: Mariko Hatta, Sc.D; Christopher I Measures, PhD.; Phoebe J Lam, PhD.; Daniel C Ohnemus, PhD.; Maureen E Auro; Maxime M Grand, PhD.; Karen E Selph, PhD.

Manuscript Region of Origin:

Abstract: The role that dissolved Fe (dFe) rich modified Circumpolar Deep Water (MCDW) might play in sustaining the frequently observed discrete patches of high chlorophyll biomass over Pennell Bank (PB) and Mawson Bank (MB) over the last 16 years in the seasonally iron (Fe)-limited waters of the Ross Sea, was investigated during a January/February 2011 cruise aboard the RV N.B. Palmer. In a 26 day period 79 stations, were sampled, some repeatedly, for hydrographic parameters on a sampling grid above and around both of these banks. Additional casts at a subset of these stations were made using a trace element clean sampling system to obtain samples for shipboard trace element determinations as well as biological incubations. Particulate sampling was accomplished at selected stations by in situ pumping and two deployments of gliders were made to assess the extended structure of the physical ecosystem. In addition a short-term mooring was located close to one of the repeat stations. The dissolved and particulate trace element results indicated that the dissolved Fe content of the Circumpolar Deep Water (CDW) is actually reduced by on-shelf mixing with Antarctic Surface Water as it transitions into MCDW. Our stations above PB, where the maximum bloom is encountered, instead showed evidence of a sedimentary input of Fe into the bottom waters, connected to the strong tidal cycles in this region, with the highest dFe values encountered when water flowed south across the large expanse of shallow sediments found on the top of this bank. While we saw no evidence of MCDW above PB, it was present above MB, the site of a smaller persistent bloom. Above MB, which also displayed the imprint of a sedimentary input, the presence of MCDW and the stronger near bottom density gradient it produces, appears to contribute to reduced vertical mixing of the sedimentary source. Thus, ironically, the presence of MCDW may be hindering the supply of Fe to the surface waters, rather than being the source, as originally hypothesized.

1 **Title:**

2 The relative roles of Modified Circumpolar Deep Water and sediment resuspension in
3 maintaining the phytoplankton blooms above Pennell and Mawson Bank, Ross Sea.

4

5 **Author names and affiliations:**

6 Mariko Hatta^{1*}, Chris. I. Measures¹, Phoebe. J. Lam^{2,3}, Daniel. C. Ohnemus^{2,4}, Maureen
7 E. Auro², Maxime. M. Grand^{1,5}, Karen. E. Selph¹

8 ¹School of Ocean and Earth Science and Technology, Department of Oceanography,
9 University of Hawai'i at Manoa, 1000 Pope Road, Honolulu, HI 96822.

10 ² Department of Marine Chemistry and Geochemistry, Woods Hole Oceanographic
11 Institution, 266 Woods Hole Road, Woods Hole, MA 02543.

12 ³ (now at) Department of Ocean Sciences, University of California, Santa Cruz, 1156
13 High St, Santa Cruz, CA 95064

14 ⁴ (now at) Bigelow Laboratory for Ocean Sciences, East Boothbay, ME, USA.

15 ⁵ (now at) Ocean and Earth Science, National Oceanography Centre Southampton,
16 University of Southampton Waterfront Campus, European Way, Southampton, SO14
17 3ZH, UK.

18 ***Corresponding author**

19 mhatta@hawaii.edu; 1-808-956-6632

20

21 **Key words (up to 6 key words):**

22 Iron; Banks; Ross Sea; Modified Circumpolar Deep Water; Water mixing; Manganese

23

24 **Highlights (3-5 highlights, 85 characters, core results):**

25 Dissolved Fe within the CDW is diluted by mixing with AASW during the formation of
26 MCDW in the Ross Sea.

27 MCDW was seen above Mawson Bank but not Pennell Bank.

28 A **sedimentary** input of Fe is seen above Pennell Bank.

29 Strong tidal energy over shallow banks brings Fe-rich deep waters to the euphotic zone.

30 The presence of MCDW above Mawson Bank hinders mixing of dFe into the euphotic
31 zone.

32

33 **Abstract:**

34 The role that dissolved iron (dFe) rich modified Circumpolar Deep Water
35 (MCDW) might play in sustaining the frequently observed discrete patches of high
36 chlorophyll biomass over Pennell Bank (PB) and Mawson Bank (MB) over the last 16
37 years in the seasonally Fe-limited waters of the Ross Sea, was investigated during a
38 January/February 2011 cruise aboard the RV N.B. Palmer. In a 26 day period 79 stations,
39 were sampled, some repeatedly, for hydrographic parameters on a sampling grid above
40 and around both of these banks. Additional casts at a subset of these stations were made
41 using a trace element clean sampling system to obtain samples for shipboard trace
42 element determinations as well as biological incubations. Particulate sampling was
43 accomplished at selected stations by *in situ* pumping and two deployments of gliders
44 were made to assess the extended structure of the physical ecosystem. In addition a
45 short-term mooring was located close to one of the repeat stations. The dissolved and
46 particulate trace element results indicated that the dissolved Fe content of the
47 Circumpolar Deep Water (CDW) is actually reduced by on-shelf mixing with Antarctic
48 Surface Water as it transitions into MCDW. Our stations above PB, where the maximum
49 bloom is encountered, instead showed evidence of a sedimentary input of Fe into the
50 bottom waters, connected to the strong tidal cycles in this region, with the highest dFe
51 values encountered when water flowed south across the large expanse of shallow
52 sediments found on the top of this bank. While we saw no evidence of MCDW above
53 PB, it was present above MB, the site of a smaller persistent bloom. Above MB, which
54 also displayed the imprint of a sedimentary input, the presence of MCDW and the
55 stronger near bottom density gradient it produces, appears to contribute to reduced
56 vertical mixing of the sedimentary source. Thus, ironically, the presence of MCDW may
57 be hindering the supply of Fe to the surface waters, rather than being the source, as
58 originally hypothesized.

59 **1. Introduction**

60 The Southern Ocean is well-known as a High Nutrient Low Chlorophyll (HNLC)
61 region, but within this low biomass area the Ross Sea continental shelf is one of the most
62 productive areas in the Southern Ocean (Sullivan et al., 1993; DiTullio and Smith, 1996;
63 Smith and Gordon, 1997; Arrigo et al., 1998a; Smith and Cosimo, 2008), and thus is
64 considered as an important oceanic CO₂ sink region (Marinov et al., 2005; Arrigo et al.,
65 1998b; Takahashi et al., 2009). The increased biomass seen during iron addition
66 experiments in the Southern Ocean waters (e.g., Martin et al., 1990; Sedwick and
67 DiTullio, 1997) suggests that it is iron, an essential nutrient for phytoplankton growth,
68 that is limiting primary production in the Southern Ocean (Martin et al., 1991; Coale et
69 al., 1996; Sedwick et al., 2000; Boyd, 2002; Coale et al., 2003; 2005; **Gerringa et al.,**
70 **2015; McGillicuddy et al., 2015**).

71 There are multiple potential iron sources to the Ross Sea, such as dust, sea-ice,
72 icebergs, upwelling of deeper waters and sedimentary input, etc., and these have been
73 discussed by a variety of authors (Martin et al., 1991; Fitzwater et al., 1996; Sedwick et
74 al., 1996; Sedwick et al., 2000; Measures and Vink, 2001; Boyd, 2002; Coale et al., 2005;
75 Sedwick et al., 2011; Measures et al., 2012; Marsay et al., 2014).

76 Seasonal iron limitation has been suggested for the Ross Sea (Sedwick and
77 DeTullio, 1997; Sedwick et al., 2000; Coale et al., 2003; 2005; Bertrand et al., 2007) as a
78 result of the effects of phytoplankton uptake, particle export, and scavenging. However,
79 in a recent study, Sedwick et al. (2011) reported low dissolved Fe (dFe) concentrations
80 (~0.1 nM) in the euphotic zone of the Ross Sea polynya by late spring (November),
81 concluding that the surface waters in the Ross Sea polynya (southern Ross Sea) can
82 become iron depleted even during an early stage of the seasonal phytoplankton bloom.
83 These authors concluded that in order to sustain the high productivity in the Ross Sea,
84 there must be a significant supply of new dFe to surface waters of the polynya during the
85 growing period.

86 **Satellite ocean colour imagery shows that** in contrast to the large areas of high
87 chlorophyll biomass in the inshore regions, the offshore regions show only small patches

88 of high chlorophyll biomass (Fig 1). In particular there are discrete blooms that have
89 been occurring above Pennell Bank (PB) and Mawson Bank (MB) at the same time of
90 year from 1998 to 2014 (Reddy and Arrigo, 2006; Kohut et al., this issue). The seasonal
91 persistence of these features also suggests that there should be a continual source of Fe,
92 fuelling phytoplankton blooms above the banks. The dye simulation model of Dinniman
93 et al. (2011) confirmed Circumpolar Deep Water (CDW) intrusions onto the shelf at
94 specific locations primarily determined by the bathymetry (Klinck and Dinniman, 2010),
95 which then mixes with surrounding water masses to become Modified Circumpolar Deep
96 Water (MCDW, Jackobs and Giulivi, 1998; Gordon et al., 2000; Orsi and Wiederwohl,
97 2009; Whitworth et al., 2013). In addition, Dinniman et al. (2011) showed there was
98 vigorous mixing of the CDW/MCDW with the surface waters in the Ross Sea. Since
99 CDW contains relatively high levels of dFe compared to the shelf region (~0.5nM at
100 65.2°S 174.7°W in the northern Ross Sea, Sedwick et al., 2011; 0.4-0.5 nM, Hoppema et
101 al., 2003; 0.51±0.16 nM, Grand et al., 2015a), this water has been considered as a
102 potential source of Fe fuelling primary production in the Ross Sea (Hiscock, 2004;
103 Peloquin and Smith, 2007).

104 The goal of our research project was to evaluate the role that Fe-enriched CDW
105 may play in fuelling these patches of higher biomass by undertaking a comprehensive
106 physical, chemical, and biological sampling program (“SEAFARERS”, Slocum
107 Enhanced Adaptive Fe Algal Research in the Ross Sea, Kohut et al., 2013) around the
108 banks during the late austral summer (Jan 2011), a time when there is no seasonal ice
109 melt to contribute to the dFe supply. To achieve this, we determined the distributions of
110 dissolved and particulate Fe, dissolved Mn and dissolved Al at key stations on the shelf to
111 enable us to follow the mixing process of CDW as it transitions into MCDW. A key
112 physical process in the Ross Sea is the strong tidal effect in this region and the tide’s
113 effect on mixing processes (Robertson et al., 2003; Whitworth and Orsi, 2006; Kohut et
114 al., 2013). To help evaluate these processes our shipboard data gathering included CTD
115 parameters from rosette casts and the ship’s acoustic doppler current profiler (ADCP).
116 Additional temperature, salinity, dissolved oxygen, fluorescence and backscatter data was
117 obtained from gliders deployed from the ship, and temperature, salinity, pressure and

118 current meter data were obtained from a mooring that was deployed at a station that was
119 occupied multiple times during the cruise (Kohut et al., this issue).

120 **2. Methods**

121 *2.1. Sampling*

122 *2.1.1 Dissolved trace metal samples*

123 Over 180 water samples were collected for trace metal determinations at 15
124 stations (Fig 1) in the Ross Sea between 17 January and 13 February 2011 as part of the
125 **SEAFARERS campaign** aboard the R/V Nathaniel B. Palmer (cruise NBP 11-01). **An**
126 **additional 12 water samples** were collected on 21 February 2011 at station 100 (Fig 1) at
127 the start of the CLIVAR S4P cruise (cruise NBP 11-02) that immediately followed the
128 cruise.

129 Water samples were obtained using a custom-built trace metal (TM) clean rosette
130 consisting of an epoxy painted Al rosette frame containing 12 x 12L GO-FLO bottles
131 (Measures et al., 2008a) and that housed an SBE 911 CTD system which included an
132 SBE 43 dissolved oxygen sensor and a Wet labs FL1 fluorometer. However, due to the
133 oxygen sensor freezing during the cruise, oxygen data are not available. Immediately
134 after each deployment the package was recovered, the tops of the GO-FLO bottles were
135 covered with plastic bags and the bottles removed from the frame and carried into **a**
136 **customized 20-foot container** van for sub-sampling (Measures et al., 2008a). The GO-
137 FLO bottles were pressurized to 10 psi using 0.2 μm -filtered compressed air and water
138 samples were filtered through 0.45 μm pore size acid washed, 47 mm polysulphone
139 filters (Pall Supor 450 P/N 60173) as they were collected into sample bottles. All sub-
140 sampling was undertaken in the clean van using rigorous trace metal protocols. The
141 sampling system and protocols are described in detail in Measures et al. (2008a).
142 Samples obtained with this system and processed in this manner have been shown during
143 the SAFe inter-comparison cruise (Johnson et al., 2007) and the GEOTRACES inter-
144 calibration cruise to produce concentrations of trace metals (Al, Fe and Mn) that are,
145 within analytical uncertainty, identical to those obtained using other currently accepted
146 sampling methodologies for trace elements (i.e., U.S. GEOTRACES sampling protocols,

147 Cutter and Bruland, 2012). Also, this sampling system has been used successfully to
148 collect uncontaminated trace element samples during several **previous** projects (e.g.,
149 CLIVAR projects: Measures et al., 2008b; Grand et al., 2014, 2015a, 2015b; BWZ
150 project: Measures et al., 2013; Hatta et al., 2013).

151 Filtered seawater samples (0.45 μm pore size) were collected and drawn into acid
152 pre-washed 125 ml polymethylpentene bottles after three rinses with sample water; filled
153 sample bottles were stored in polyethylene bags in the dark at room temperature before
154 the shipboard determination. Duplicate samples were also collected and drawn into
155 previously acid-leached 125 mL HDPE bottles after three sample rinses for shore-based
156 determination of dissolved Fe (dFe) and dissolved Mn (dMn) by Inductively Coupled
157 Plasma Mass Spectrometry (ICP-MS).

158 ***2.1.2 Particulate Fe samples***

159 Size-fractionated **particles for particulate Fe determination were collected from 6**
160 **depths** at selected stations (Stations 14, 55, 70, 35, 24, 7, and 28, shown in Fig 1) by in-
161 situ filtration using modified dual-flow McLane WTS pumps (Ohnemus and Lam, 2015).
162 **Pumps were clamped onto non-metallic Hytrel-jacketed Vectran wire.** The filter
163 configurations on the two flowpaths were those used on all US GEOTRACES cruises,
164 and consisted of a 51 μm polyester prefilter followed by paired 0.8 μm polyethersulfone
165 (PES; Pall Supor800) filters “Supor”, and a 51 μm polyester prefilter followed by paired
166 quartz fiber filters “QMA” (Whatman QMA) (Cutter et al., 2014; Ohnemus and Lam,
167 2015). **All filters were 142 mm in diameter, and had an active filtering diameter of 126**
168 **mm.** Up to 478 L and 1100 L were filtered through the “Supor” and “QMA” flowpaths,
169 respectively, over the typical 2-3 hour pump time at an initial pumping rate of 8 L/min.
170 A complete filter set sandwiched between 1 μm mesh in perforated polypropylene
171 containers was deployed at each station as a “dipped blank”, which functioned as a
172 process and adsorption blank.

173 ***2.2 Analytical methods***

174 ***2.2.1 Determination of dissolved trace elements***

175 Dissolved trace element determinations were performed on board ship using the
176 filtered sub-samples from the GO-FLO bottles within a few hours of sample collection.
177 Prior to analysis, samples were acidified by adding 125 μL sub-boiling distilled 6N HCl,
178 and were then heated in groups of 4 for 3 minutes in a 900 W microwave oven to achieve
179 a temperature of $60 \pm 10^\circ\text{C}$, to release dFe from complexation in the samples. Samples
180 were allowed to cool to room temperature for at least 1 hour prior to Flow Injection
181 Analysis (FIA). The same method was used in a previous study (Hatta et al., 2015).

182 Dissolved Al (dAl), dFe and dissolved Mn (dMn) were determined in the filtered,
183 acidified, microwave-treated subsamples using FIA methods of Resing and Measures
184 (1994) for Al, Measures et al. (1995) for dFe, and Resing and Mottl (1992) for dMn
185 determinations. The detection limits were 0.40 nM dAl, 0.06 nM dFe, and 0.19 nM dMn.
186 However, since most of the results from the shipboard dMn analysis were below the
187 shipboard detection limit, we use dMn data from the duplicate samples determined in the
188 more sensitive shore-based ICP-MS at the University of Hawaii in this study. The Al and
189 Fe data presented here are from the shipboard FIA determinations.

190 Shipboard data sets have been compared with the ICP-MS data to calculate the
191 FIA system blank for dFe. No detectable blank from either the acid or sample buffer
192 were found for Al. Samples for shore-based ICP-MS determinations for dFe and dMn
193 were filtered on board using identical methods as those for the FIA samples, and were
194 stored in 125 mL LDPE bottles and acidified in the shore lab to 0.024 M with ultrapure
195 6N HCl, prior to analysis. Pre-concentration and extraction of samples for the
196 determination of dFe and dMn was performed using a flow injection manifold with an in-
197 line micro-column containing $\square 200 \mu\text{L}$ of Toyopearl AF Chelate-650 M resin following
198 the protocol of Milne et al., (2010). The pre-concentrated samples were analyzed by
199 ICP-MS (Element2, Thermo Scientific) with an Apex-Q (ESI). Detection limits for Fe
200 and Mn were calculated from 3 standard deviations of determinations of replicate ICP-
201 MS measurements and were approximately 0.01 nM and 0.05 nM, for Fe and Mn,
202 respectively. Determination of dFe ($1.00 \pm 0.14 \text{ nM}$, $n=10$) in the GEOTRACES open
203 ocean reference material (GD) were in good agreement with the inter-laboratory averages
204 reported for these materials ($\text{GD} = 0.95 \pm 0.05 \mu\text{mol/kg}$). Determination of dMn ($0.23 \pm$

205 0.03 nM, n=10 (GD); 1.30 ± 0.39 nM, n=5 (GS)) in the GEOTRACES open ocean
206 reference material were also in good agreement with the inter-laboratory averages
207 reported for these materials (GD = 0.21 ± 0.04 $\mu\text{mol/kg}$, GS = 1.45 ± 0.17 $\mu\text{mol/kg}$).

208 **2.2.2 Determination of particulate trace metals**

209 Separate subsamples of the top Supor filter (the 0.8 - 51 μm size fraction)
210 representing 3 - 9% of the filter area (median 13 L equivalent volume filtered) were used
211 to determine the total and leachable concentrations of particulate trace metals. Total
212 digestions were effected with the Piranha method (Ohnemus et al., 2014; Ohnemus and
213 Lam, 2015). Briefly, this two-step digestion first uses a strong oxidizing solution (the
214 Piranha reagent: 3 parts concentrated H_2SO_4 to 1 part concentrated H_2O_2) to completely
215 digest the PES filter and other particulate organic material, followed by a strong acid
216 cocktail (4M each of HNO_3 , HCl , and HF) to completely digest the silicate components
217 of suspended marine particles. For acid **leachable** concentrations of particulate trace
218 metals, separate subsamples were leached in 2 mL 1M HCl at room temperature for 24
219 hours in 15 mL centrifuge tubes. Samples were centrifuged at 4100 rpm for 45 minutes,
220 and 1.5 mL of supernatant was transferred into a Teflon vial. The cold HCl leach used
221 here is more aggressive than other commonly used weak acid leaches (e.g., Berger et al.,
222 2008), but **is similar to weak acid leaches frequently used on size-fractionated in-situ**
223 **pump samples (Bishop et al., 1977; Lam et al., 2006; Lam and Bishop., 2008), and** has
224 the advantage of having been tested on a variety of iron bearing minerals: it has been
225 shown to extract Fe from poorly crystalline Fe(III) oxyhydroxides and a small fraction of
226 some phyllosilicates, but not crystalline Fe(III) oxides (Raiswell et al., 1994).

227 Total digest and leach solutions were dried down at 110 $^\circ\text{C}$ and residues were
228 brought back up into solution with 5% HNO_3 . The final solution was run at the **Woods**
229 **Hole Oceanographic Institution (WHOI)** Plasma facility on a Thermo Element2 HR ICP-
230 MS using a quartz spray chamber introduction system. Matrix suppression and internal
231 drift was corrected using 1 ppb In as an internal standard, and concentrations were
232 quantified using mixed element external standard curves (Ohnemus et al., 2014). The
233 detection limit was defined as three times the standard deviation of all dipped blank
234 filters, and was 2.7 nmol/filter and 9.9 nmol/filter for leachable and total particulate Fe

235 (pFe), respectively. For a median volume filtered of 300 L, this is equivalent to detection
236 limits of 9 pM for leachable pFe and 33 pM for total pFe. Repeat determinations of total
237 and leachable pFe had average relative standard deviations of 3% and 10%, respectively.

238 *2.3 Ancillary data*

239 In order to understand the detailed water characteristics and biological activity
240 during the cruise, shipboard ADCP data, oxygen data, photosynthetically active radiation
241 (PAR) data, and fluorescence data are used in the discussion. However, since there was
242 no PAR sensor or transmissometer sensor attached to the TM rosette and no usable data
243 from the TM rosette oxygen sensor, we use oxygen, and PAR data from the regular
244 hydrographic CTD rosette casts, which were deployed within 2-3 hours of the TM casts.
245 Temperature and salinity records indicated that there was no significant change in water
246 properties between these occupations (data not shown).

247 **ADCP data (units: m/s):** In order to identify the surface currents and tidal
248 influence during the sampling period, we use the shipboard hull-mounted ADCP
249 “narrowband” instrument (NB150). These data are publicly available at the website
250 <http://currents.soest.hawaii.edu/nbpalmer/> using the cruise recognition code of
251 “nbp1101”.

252 **Fluorescence (units: volts):** The raw sensor voltages (0-5 volts) from the Wet
253 Labs FLRTD-855 (mounted on the TM rosette during each cast) are used in this study.

254 **Mixed layer depth (units: m):** The oceanic mixed layer is defined as the surface
255 layer where the temperature and salinity are vertically homogeneous. In the Southern
256 Ocean, Mixed Layer Depths (MLDs) have previously been defined using criteria based
257 on the change in potential temperature or density with respect to the surface value, (e.g.,
258 $\Delta\theta = 0.5^\circ\text{C}$, $\Delta\sigma_\theta = 0.125 \text{ kg/m}^3$ and $\Delta\theta = 0.2^\circ\text{C}$, $\Delta\sigma_\theta = 0.03 \text{ kg/m}^3$). In this study, we
259 define the MLDs using the potential density criteria of $\Delta\sigma_\theta = 0.03 \text{ kg/m}^3$ from the surface
260 value, which has also been shown to provide good agreement between density and
261 oxygen based mixed layers in the Bellingshausen Sea (Castro-Morales and Kaiser, 2012).
262 Calculated MLDs (data from regular hydrography CTD rosette and TM rosette) and the

263 depth of the PAR 1% light level are shown in Table 1 together with selected water
264 property parameters within the **mixed layer**.

265 **3. Results and discussion**

266 Here we report the dissolved ($<0.45 \mu\text{m}$) Al, Fe, Mn from the trace metal clean
267 rosette sampling system and the particulate (leachable and total) Fe data from the **in-situ**
268 pumping system. All of the trace metal data presented here are available at the U.S.
269 Antarctic Program Data Center using Entry ID: NBP1101.
270 [http://gcmd.nasa.gov/KeywordSearch/Metadata.do?Portal=GCMD&MetadataView=Full](http://gcmd.nasa.gov/KeywordSearch/Metadata.do?Portal=GCMD&MetadataView=Full&EntryId=NBP1101)
271 [&EntryId=NBP1101](http://gcmd.nasa.gov/KeywordSearch/Metadata.do?Portal=GCMD&MetadataView=Full&EntryId=NBP1101).

272 Potential temperature and salinity data are shown in Fig 2 with selected stations
273 shown in color in order to identify typical water masses found in the study area. The
274 distribution of hydrographic parameters (temperature, salinity, neutral density,
275 fluorescence, silicate, and phosphate) in the section across the basin (red box shown in
276 Fig 1) are shown in Fig 3, and the corresponding dissolved and particulate trace metal
277 distributions are shown in Fig 4. The vertical depth profiles of hydrographic parameters
278 and trace elements at the repeated sampling station located on the western side of PB in
279 Joides Basin and the offshore station are presented in Fig 5 and data from the stations
280 above PB and MB are in Fig 6. Property-property plots of the MCDW (neutral density =
281 $28.0 - 28.27 \text{ kg/m}^3$) are shown in Fig 7. Figures were made using Ocean Data View
282 (Schlitzer, 2015). The MLDs at each station are shown in Table 1, and the averaged
283 concentration of each dissolved parameter in the each of the water masses are shown in
284 Table 2. The pFe values (leachable and total) in each water mass are shown in Table 3.

285 **3.1 Water mass characteristics of the Ross Sea**

286 Across the sampling region, the presence of Antarctic Surface Water (AASW),
287 neutral density $<28.00 \text{ kg/m}^3$ (Orsi and Wiederwohl 2009), is evident in the upper 200 m
288 from its high temperature and low salinity. **Below 300 m, in the channels between the**
289 **banks, shelf waters (neutral density $>28.27 \text{ kg/m}^3$, Orsi and Wiederwohl, 2009) can be**
290 **seen as High Salinity Shelf Water (HSSW, $>34.62 \text{ psu}$) at stations 2, 24, 55 & 100, and**
291 **Low Salinity Shelf Water (LSSW, $<34.62 \text{ psu}$) at station 3 (Fig 2).** Between these water

292 masses lies the MCDW, which results from mixing of the inflowing CDW with AASW
293 as it flows southward across the shelf. This MCDW, neutral density 28.00 - 28.27 kg/m³
294 (Orsi and Wiederwohl 2009; Kohut et al., 2013), can be seen along the western side of
295 PB at 218 - 275 m (Stations 16, 24, 41) and along the western side of MB at 150 - 230 m
296 (Station 55). This water mass has a relatively high temperature (-1.3 to -0.6 °C), low
297 salinity (34.52 - 34.55 psu) and low dissolved oxygen (DO; 233 - 250 µmol/kg, latter not
298 shown in this figure) as a result of the properties of the originating offshore CDW.

299 **3.2 Dissolved and particulate trace metal distributions**

300 The trace element distributions show large contrasts, with low concentrations in
301 surface waters and higher concentrations towards the bottom (Fig 4). The following
302 sections will focus on each water mass as identified by its physical properties discussed
303 above. We will first look at the characteristics of the two potential mixing partners of
304 CDW, i.e., the surface waters (AASW) and the deeper waters (HSSW), before using this
305 information to describe the evolution of the MCDW on the shelf.

306 **3.2.1 Surface Waters (AASW) in the mixed layer**

307 Our measured surface dFe values (0.08 - 0.25 nM, Table 2) are similar to the
308 concentrations in surface water found during summer 1995 (0.18 ± 0.08 nM, Sedwick et
309 al., 2000), and are slightly higher than the recently reported results in open polynya
310 surface waters further to the south of our region (0.10 ± 0.05 nM in 2005-2006 summer,
311 0.06 ± 0.04 nM in 2006 spring, Sedwick et al., 2011; and 0.08 ± 0.07 nM in 2012
312 summer, Marsay et al., 2014).

313 Shipboard Fe-addition incubation experiments strongly suggested that all the
314 surface waters of the region were deficient in dFe (Kustka et al., 2015) at the time of our
315 later summer cruise. However, we observed persistent patches of high fluorescence (i.e.,
316 greater phytoplankton blooms), as discussed in the introduction, at Station 35 and over
317 PB at Stations 7, 61 and 28 where fluorometer signals were >0.82 volts, there was also an
318 additional, weaker, patch of high fluorescence at Station 48. These patches corresponded
319 to higher surface temperature, lower silicate and phosphate concentrations (Fig 3a, e, f),

320 slightly higher dFe values (0.15-0.25 nM) and higher concentrations of leachable and
321 total pFe (Table 3).

322 In contrast surface waters with lower fluorescence (<0.4 volts, Stations 55, 70, 16,
323 and 41) had relatively lower dFe values (0.08-0.17 nM). In an Fe-limited region it would
324 be expected, on a steady-state basis, that lower concentrations of dFe would be coincident
325 with higher biomass, since biological uptake would be rapidly removing any biologically
326 available Fe from the dissolved to the particulate phase. However, this is an extremely
327 dynamic region with strong tides and topographically induced mixing, thus unlikely to be
328 at steady state. The observation of higher dFe concentrations in places of enhanced
329 biomass is consistent with a location where there is a continuous supply of Fe to surface
330 waters which exceeds the biological removal rate. The vertical profiles of pFe and dFe
331 above PB suggest that there is a potential sedimentary source of leachable pFe and dFe,
332 to the upper water column above the banks. We note that at the elevated fluorescence
333 sites a significant portion of the higher surface pFe is refractory (%leachable < 40%) and
334 thus presumably of sedimentary origin, which implies a sufficiently vigorous mixing
335 process to supply sedimentary derived pFe and dFe to surface waters which we postulate
336 supports the enhanced growth of phytoplankton in these places.

337 **3.2 Shelf Water and Modified Shelf Waters**

338 At the bottom of the profiles during the outflowing tide (northward flow), we
339 found Shelf Waters (HSSW and LSSW) at Stations 2 & 3 (inner shelf), 24 & 100 (JB),
340 and 55 (DB). In contrast, we do not find these water masses during the incoming
341 (southward flow) when the deepest waters are much warmer and fit the Modified Shelf
342 Water (MSW) definition of Orsi and Weidnerwohl (2009). At the stations that contain
343 HSSW and LSSW we see dFe and dMn concentrations continually increasing in the
344 bottom ~100 m towards the deepest sample ~30 m above the sediments. The
345 concentrations of dAl also increase at most of these stations except for station 3 which
346 interestingly is the only one with LSSW in the deepest water. Where available, pFe
347 values (both total and leachable) are also high and increase towards the sediments in the
348 deep waters at stations 55 and 24, but those samples were not collected as close to the
349 bottom as the dissolved samples. We take this as evidence of a common benthic source

350 for these elements probably as a result of the release of pore waters from the sediments or
351 perhaps remineralization of material within the benthic nepheloid layer supported by the
352 strong tidal action on the shelf. This would be similar to the observations reported by
353 Hatta et al. (2013), for the Bransfield Strait region. Additional support for this idea
354 comes from Marsay et al. (2014), who recently reported a high benthic flux of dFe from
355 the sediments in the southern part of Ross Sea continental shelf during the austral
356 summer 2012.

357 **3.3 Modified Circumpolar Deep Water (MCDW)**

358 In order to understand the evolution of the MCDW as it flows across the shelf,
359 water samples were collected repeatedly at different stages of the tidal cycle at a location
360 in the Joides Basin to the west of PB over an 11-day period (Stations 16, 24, 41, shown in
361 Fig 1). The dFe profiles during all three occupations show **consistent values** (0.1 - 0.2
362 nM) from the surface to 200 m in the AASW (Fig 5b). Below the AASW is the depth of
363 the core of the MCDW (shown by the coloured star symbol * at each station and defined
364 by a neutral density range of 28.00 - 28.27 kg/m³, Fig 5). The core of the MCDW, which
365 varies in depth between the occupations as a result of the tidal cycle, is coincident with
366 the depth where Fe concentrations start to increase, but the pattern of increase is different
367 between occupations **over** the tidal cycle. At Stations 16 and 41, dFe values within the
368 deeper core are 0.27 - 0.33 nM, while at Station 24 (with a shallower MCDW core) dFe
369 values continually increase from 0.27 nM at 220 m to 0.64 nM at the bottom where
370 HSSW is found (>34.62 psu, Fig 5d). The end member CDW was sampled at the
371 offshore Station 14, where dFe values **range from 0.33 nM at 400 m to 0.42 nM at 1,000**
372 **m (average 0.36 nM, Table 2)**. It should be noted that the CDW found here had a
373 **maximum potential temperature of 1.3°C and a salinity of 34.71**, indicating that while it
374 **is in the fairly broad range of the classical values of CDW (Emery and Meincke, 1986) of**
375 **0.1-2°C and 34.62-34.73 salinity**, there may have been local modification of this water
376 **mass near the shelf edge (Orsi and Weiderwohl. 2009)**.

377 The shipboard ADCP data during the sampling period of each sampling station
378 (~2 hours), **along with the mooring data**, shows the importance of the relative motion of
379 the water across the shelf (Kohut et al., 2013). There was southward (onshore) flow

380 during the occupation of Stations 16 (-0.32 ± 0.03 m/s) and 41 (-0.15 ± 0.05 m/s) and
381 northward (offshore) flow during the occupation of Station 24 ($+0.12 \pm 0.04$ m/s). These
382 flow patterns suggest that the deepwater increase in dFe value at Station 24 is from
383 outflowing HSSW shelf waters, which were enriched from benthic sources further south
384 driven by strong tidal processes. The MSW present at the base of Stations 16 and 41 is
385 much more dilute in dFe, with lower salinity and higher temperatures corresponding to a
386 very small increase in dFe in the bottom-most samples. In contrast, at Station 16, there is
387 a higher dFe value in the MCDW compared to Station 41, which corresponds to stronger
388 onshore flow of the dFe-enriched CDW source (Fig 5b).

389 MCDW is also seen in the deeper channels at Stations 55, 35, 100, 28, the inner
390 shelf at Station 2, and on top of MB at Station 70. As we will argue below, the relative
391 concentration of dFe in the MCDW at these stations appears to be controlled mainly by
392 how much mixing the original CDW has undergone.

393 We will use water mass properties to examine the origin of the trace metal signals
394 in the MCDW. A property-property plot of salinity and potential temperature (within the
395 neutral density range of MCDW) suggests that MCDW is formed by mixing the CDW
396 end member with a low salinity end member, i.e., ASSW rather than higher salinity
397 HSSW (Fig 7a). Although Si is not a conservative parameter, this concept is supported
398 by the salinity vs. Si plot, which also indicates a low Si, low salinity ASSW source rather
399 than the higher Si, higher salinity HSSW (Fig 7b). Similarly, the dFe (also not
400 conservative) vs. salinity plot also shows a low dFe mixing partner for the CDW rather
401 than the high dFe HSSW source (Fig 7c). In addition, the dAl and dMn show this same
402 mixing series, but less clearly (Fig 7d, e). Thus, the formation of MCDW from CDW
403 results, at this time of year, in a decrease of its dFe content, thus limiting its ability to
404 support biological production. The plot of dFe and dMn in the MCDW (Fig 7f) also
405 confirms the end member mixing series between the high Fe, low Mn CDW and the low
406 Fe, high Mn AASW. Since the Fe and Mn in the AASW probably have a similar
407 sedimentary source, the fractionation between these two tracers is presumably a result of
408 the shorter residence time of dFe compared to that of dMn in the AASW.

409 In contrast, the leachable pFe values of MCDW (0.93 nM at 230 m at Station 55,
410 and 1.01 nM at 210 m at Station 24, Table 3) are one order of magnitude higher than
411 those in the CDW (e.g., 0.075 nM at offshore Station 14). Additionally, the total pFe
412 values of MCDW (2.75 nM at Station 55 and 3.07 nM at Station 24) are one order of
413 magnitude higher than total pFe in the CDW (0.213 nM at Station 14). This suggests that
414 the MCDW is gaining pFe when it flows onto the shelf, but the dFe is not changing
415 **significantly during this process**. In contrast, the dMn value of MCDW (0.34 – 0.58 nM)
416 is higher than in the CDW (0.11 nM). The opposite behavior of these two dissolved
417 components is consistent with the MCDW being a mixture between the high Fe, low Mn
418 CDW and a low Fe, high Mn AASW (Fig 7c, d, f and Table 2). Also, this suggests that
419 this MCDW is probably not mixed with the HSSW that contains the highest dFe values at
420 Station 24 in the trough on the western side of PB.

421 **3.4 The waters above Pennell Bank**

422 Repeat water samples were collected **18 days apart** at one station above PB
423 (Stations 7 and 61) and samples were also obtained at Station 48 located to the north of
424 these stations within the same period (Fig 6). As mentioned before, at Stations 7 and 61,
425 the slightly higher dFe (0.15 nM and 0.25 nM, respectively, shown in Table 2) were seen
426 coincident with higher fluorescence signals (1.73 and 1.66 volts, respectively). In
427 contrast, the lower dFe values (0.13 nM) were seen in the upper 50 m at Station 48 where
428 there was a relatively low fluorescence signal (0.48 volts).

429 At each of these stations, the dissolved trace element signals are higher below 170
430 m than in the surface waters, suggesting a benthic input (Fig 6b, c). **We note that all the**
431 **water above PB is AASW including the deepest water which has neutral densities (27.99**
432 **- 28.03 kg/m³) that are less than, or at the very edge of, the definition of the classic**
433 **MCDW (28.00 - 28.27 kg/m³) thus the AASW properties are not a result of mixing with**
434 **CDW/MCDW**. Below 170 m, Station 7 shows constant dFe (0.22 ± 0.01 nM) and dMn
435 (0.37 ± 0.03 nM) values, while Station 48 (dFe = 0.22 to 0.27 nM; dMn = 0.50 to 0.70
436 nM) and Station 61 (dFe = 0.20 to 0.36 nM; dMn = 0.69 to 0.90 nM) show gradual
437 increases from ~170 m to the bottom (Fig 6b). These features, however, are more
438 pronounced at Station 61 and 48 than at Station 7. Interestingly, shipboard ADCP data

439 during each sampling period (averaged over ~2 hours) shows northward flow (off shelf)
440 during the occupation of Station 7 ($+0.14 \pm 0.03$ m/s), while there is no strong flow
441 during the occupation of Station 48 (-0.042 ± 0.04 m/s) and Station 61 ($+0.001 \pm 0.04$
442 m/s). Thus, during the occupation of Station 7, under tidal influence, the deepest waters
443 were moving northward on to the PB from deeper areas to the south. In contrast, during
444 the occupation of Stations 48 and 61, the tide was fairly slack, i.e., little motion, but prior
445 to the sampling the water had been moving south across the shallow area of Pennell
446 Bank. It thus seems from our profiles that when the bottom waters move south across the
447 shallower parts of the bank dissolved Fe and Mn are added to the water column.
448 However, when that water moves north onto the bank, it has not had a significant benthic
449 input before reaching the southern edge of the bank. In addition, the salinity below 150
450 m at Station 48 is very uniform (Fig 6d), suggesting that there may be topographically-
451 induced mixing of the bottom waters in this region to the north of the location of Stations
452 7 and 61. While we do have total and leachable pFe from Station 7 showing increases in
453 both loads towards the sediment interface, we do not have equivalent data from Stations
454 48 and 61. Since there is no presence of MCDW the elevated Fe seen in the AASW here
455 is not a result of MCDW, but from a local sedimentary input. The increase in dMn
456 values in the bottom waters also suggests a sedimentary input, since MCDW has a lower
457 dMn than AASW.

458 3.5 The waters above Mawson Bank and comparison to Pennell Bank

459 In contrast to PB, there is a distinct signal of MCDW at Station 70 above MB
460 between 150 m and the bottom at 255 m (neutral density $28.04 - 28.06$ kg/m³). Within
461 this water mass, we see dFe of 0.28 nM (Table 2), similar to that seen at the repeat
462 stations in the Joides Basin along the western side of PB. However, we do not see any
463 increase in dFe at the very bottom of the profile, suggesting either a lack of diagenetic
464 input or its masking by the relatively elevated dFe present in the MCDW (Fig 6b).
465 Although there appears to be a greater potential supply of dFe in the deeper water column
466 above MB than PB, and a greater potential supply of leachable pFe (Fig 6f), the biomass
467 accumulation is greatest above PB. If, as mentioned earlier, all of the surface waters of
468 the region are Fe-limited, then this suggests that the rate at which these deep supplies of

469 dFe are reaching the euphotic zone must be the factor controlling biological processes in
470 the surface waters. We note that the density gradient in the water column above MB is
471 much greater than that above PB, largely as a result of the presence of more salty MCDW
472 above MB. In fact, calculation of the Brunt Vaisala frequency (Fig 6f) reveals a uniform
473 value of <0.8 cycles/hr in the bottom 80 m layer, coincident with the presence of MCDW
474 over MB, but a gently increasing value from 0.5 to 1.8 cycles/hr in the 80 m bottom layer
475 over PB. This gradient suggests significant inhibition to mixing of the bottom layer over
476 MB, but less over PB, and it is consistent with a similar and more complete analysis of
477 mixing presented by Kohut et al. (this issue). In contrast, the deep water immediately
478 above PB is comprised of AASW and has much smaller salinity gradients, so presumably
479 experiences less hindrance to vertical mixing of this putative benthic source.

480 **4. Conclusion**

481 Dissolved Fe (dFe) values within MCDW (neutral density of 28.00 - 28.27 kg/m³)
482 to the west of PB during different stages of the tidal cycle show that the dFe content
483 within the CDW is diluted by AASW during its evolution into MCDW.

484 The bottom waters above PB, with neutral densities of 27.99 - 28.03 kg/m³, are
485 less than or at the very edge of the definition of the classic MCDW. The bottom waters,
486 however, show a diagenetic input of Fe and Mn as a result of tidal mixing and
487 topographic forcing, over the large area of shallow sediments on this bank. This input is
488 most pronounced when the water has flowed across the bank from the north rather than
489 when it enters from the south.

490 In contrast, the bottom water above MB (neutral densities of 28.04 -28.06 kg/m³)
491 has a sizeable supply of dFe and pFe associated with the presence of MCDW, but there
492 does not appear to be a diagenetic input into the deep waters here.

493 The fact that there is less biomass in surface waters, but more dFe in deep waters
494 above MB, compared to more biomass in surface waters, but less dFe in deep waters
495 above PB, suggests that there is more limited upward mixing of deep waters above MB
496 (and thus less upward mixing of dFe) as a result of the greater density gradient from salty
497 MCDW in the water column on this bank. Thus, ironically, MCDW may be hindering

498 the supply of Fe to the surface waters, rather than being the source of this limiting micro-
499 nutrient, as originally hypothesized.

500 **Acknowledgements**

501 We thank the Captain and crew of the RV NB Palmer and the RPSC technical
502 support staff both on land and at sea for their professional help in planning and ensuring a
503 successful expedition in Ross Sea. We also thank our fellow scientists for their frequent
504 help in the sub-sampling program and TM casts during the cruise, and the chief scientist
505 Dr. Kohut and co-chief scientist Dr. Kustka and other PIs for making their data available
506 and compiling the cruise data sets. Finally, we thank Dr. Swift (chief scientist) and the
507 CLIVAR group for allowing us to occupy an extra station **during the following CLIVAR**
508 **S4P cruise, which had been lost to bad weather, during the SEAFARERS cruise.**

509 We also thank the National Science Foundation for its financial support of this
510 project through Office of Polar Programs Grant numbers ANT-0839024 to CIM and
511 ANT-0838921 to PJJ. This is contribution no. **XXXX** of the School of Ocean Earth
512 Science and Technology, University of Hawaii.

513

514 **References**

- 515 Arrigo, K.R., A. M. Weiss, and W.O. Smith Jr., 1998a, Physical forcing of phytoplankton
516 dynamics in the southern western Ross Sea, *J. Geophys. Res.*, 103, 1007-1021, DOI:
517 10.1029/97JC02326.
- 518 Arrigo, K.R., D. Worthen, A.Schnell and M.P. Lizotte, 1998b. Primary production in
519 Southern Ocean waters, *J. Geophys. Res.*, 103, 15587-15600, DOI:
520 10.1029/98JC00930.
- 521 Berger, C.J.M., Lippiatt, S.M., Lawrence, M.G., Bruland, K.W., 2008. Application of a
522 chemical leach technique for estimating labile particulate aluminum, iron, and
523 manganese in the Columbia River plume and coastal waters off Oregon and
524 Washington. *J. Geophys. Res.* 113, C00B01. 10.1029/2007jc004703.
- 525 Bertrand, E. M., M.A. Saito, J. M. Rose, C.R. Riesselman, M.C. Lohan, 2007. A.E.
526 Noble, P.A. Lee, and G.R. DiTullio, Vitamin B12 and iron colimitation of
527 phytoplankton growth in the Ross Sea., *Limnol. Oceanogr.* , 52, 1079-1093,
528 doi:10.4319/lo.2007.52.3.1079.
- 529 Bishop, J.K.B., Edmond, J.M., Ketten, D.R., Bacon, M.P., Silker, W.B., 1977. Chemistry,
530 Biology, and Vertical Flux of Particulate Matter from Upper 400 M of Equatorial
531 Atlantic Ocean. *Deep-Sea Research* 24 (6), 511-548.
- 532 Boyd, P.W. 2002. Environmental factors controlling phytoplankton processes in the
533 Southern Ocean, *J. Phycol.*, 38. 844-861. Doi:10.1046/j.1529-8817.2002.t01-1-
534 01203.x.
- 535 Castro-Morales, K., and J. Kaiser., 2012. Using dissolved oxygen concentrations to
536 determine mixed layer depths in the Bellingshausen Sea. *Ocean Science* 8, 1-10,
537 doi:10.5194/ox-8-1-2012.
- 538 Coale, K.H., 1991. Effects of iron, manganese, copper, and zinc enrichments on
539 productivity and biomass in the subarctic Pacific, *Limnology and Oceanography* 36,
540 1851-1864. DOI: 10.4319/lo.1991.36.8.1851.
- 541 Coale, K.H., et al.1996. A massive phytoplankton bloom induced by ecosystem-scale
542 iron fertilization experiment in the equatorial Pacific Ocean, *Nature*,383, 495-501,
543 doi:10.1038/383495a0.

544 Coale, K. H., X. J. Wang, S. J. Tanner, and K. S. Johnson. 2003. Phytoplankton growth
545 and biological response to iron and zinc addition in the Ross Sea and Antarctic
546 Circumpolar Current along 170°W. *Deep Sea Research Part II* 50:635–653,
547 doi:10.1016/S0967-0645(02)00588-X.

548 Coale, K. H., R. M. Gordon, and X. Wang. 2005. The distribution and behavior of
549 dissolved and particulate iron and zinc in the Ross Sea and Antarctic circumpolar
550 current along 170°W, *Deep Sea Res., Part I.* 52, 295-318,
551 doi:10.1016/j.dsr.2005.09.008.

552 Cutter, G.A., Andersson, P., Codispoti, L., Croot, P., Francois, F., Lohan, M.C., Obata,
553 H., Rutgers van der Loeff, M., 2014. Sampling and Sample-handling Protocols for
554 GEOTRACES Cruises, v2.0.
555 <http://geotraces.org/images/stories/documents/intercalibration/Cookbook.pdf>.

556 Cutter, G., and K. W. Bruland. 2012. Rapid and noncontaminating sampling system for
557 trace elements in global ocean surveys. *Limnology and Oceanography: Methods* 10:
558 425–436, doi:10.4319/lom.2012.10.425.

559 Dinniman, M.S., Klinck, J.M., W.O. Smith Jr., 2011. A model study of Circumpolar
560 Deep Water on the West Antarctic Peninsula and Ross Sea continental shelves.
561 *Deep-Sea Research II* 58. 1508-1523, doi:10.1016/j.dsr2.2010.11.013.

562 DiTullio, G.R., and W.O. Smith Jr., 1996. Spatial patterns in phytoplankton biomass and
563 pigment distributions in the Ross Sea. *J. Geophys. Res.*,101. 18467-18477, DOI:
564 10.1029/96JC00034.

565 Emery, W.J., and J. Meincke, 1986. Global water masses: summary and review, *Oceanol.*
566 *acta*, 9 (4), 383-391.

567 Fitzwater, S.E., K.S. Johnson, R.M. Gordon, and K.H. Coale, 1996. Iron and zinc in the
568 Ross Sea, 1990 (abstract), *Eos Trans. AGU*, 76(3), Supplement, AGU-ASLO Ocean
569 Sci. Meet. Suppl., pg. OS192.

570 Gerringa, L.J.A., P. Laan, G.L. van Dijken, H. van Haren, H.J.W. De Baar, K.R. Arrigo,
571 A.-C. Alderkamp, 2015. Sources of iron in the Ross Sea Polynya in early summer,
572 *Marine Chemistry*, 177, 447-459, doi:10.1016/j.marchem.2015.06.002.

573 Gordon, L., I., L.A. Codispoti, J. C. Jennings Jr., F.J. Millero, J.M.Morrison, and C.
574 Sweeney, 2000. Seasonal evolution of hydrographic properties in the Ross Sea,
575 Antarctica, 1996-1997, *Deep Sea Res., Part II*, 47, 3095-3117, doi:10.1016/S0967-
576 0645(00)00060-6.

577 Grand, M.M., C.S. Buck, W.M. Landing, C.I. Measures, M. Hatta, W.T. Hiscock,
578 M. Brown, and J.A. Resing. 2014. Quantifying the impact of atmospheric
579 deposition on the biogeochemistry of Fe and Al in the upper ocean: A decade of
580 collaboration with the US CLIVAR-CO2 Repeat Hydrography Program.
581 *Oceanography* 27(1):62–65, <http://dx.doi.org/10.5670/oceanog.2014.08>.

582 Grand, M. M., C. I. Measures, M. Hatta, W. T. Hiscock, C. S. Buck, and W. M. Landing
583 (2015a), Dust deposition in the eastern Indian Ocean: The ocean perspective from
584 Antarctica to the Bay of Bengal, *Global Biogeochem. Cycles*, 29,
585 doi:10.1002/2014GB004898.

586 Grand, M. M., C. I. Measures, M. Hatta, W. T. Hiscock, W. M. Landing, P. L. Morton, C.
587 S. Buck, P. M. Barrett, and J. A. Resing (2015b), Dissolved Fe and Al in the
588 upper 1000 m of the eastern Indian Ocean: A high-resolution transect along 95°E
589 from the Antarctic margin to the Bay of Bengal, *Global Biogeochem. Cycles*, 29,
590 doi:10.1002/2014GB004920.

591 Hatta, M., Measures, C.I., Selph, K.E., Zhou, M., Hiscock, W.T. 2013. Iron fluxes from
592 the shelf regions near the South Shetland Islands in the Drake Passage during the
593 austral-winter 2006, *Deep-Sea Res. II*. 90. 89-101.

594 Hatta, M., Measures, C.I., Wu, J., Roshan, S., Fitzsimmons, J.N., Sedwick, P., Morton, P.
595 2015. An overview of dissolved Fe and Mn distributions during the 2010–2011
596 U.S. GEOTRACES north Atlantic cruises: GEOTRACES GA03. *Deep Sea Res*
597 *II*. 116, 117-129. doi:19.1916/j.dsr2.2014.07.005.

- 598 Hiscock, M.R., 2004. The regulation of primary productivity in the Southern Ocean, PhD
599 Dissertation, Duke University, 150pp.
- 600 Hoppema, M., H. J. W. de Baar, E. Fahrback, H. H. Hellmer, and B. Klein (2003),
601 Substantial advective iron loss diminishes phytoplankton production in the
602 Antarctic Zone, *Global Biogeochem. Cycles*, 17(1), 1025,
603 doi:10.1029/2002GB001957.
- 604 Jackobs, S.A., and C.F.Giulivi, Interannual ocean and sea ice variability in the Ross Sea.
605 1998. In *Ocean, Ice, and atmosphere: Interactions at the Antarctic Continental*
606 *Margin*, edited by S.S. Jacobs, and R.F. Weiss, pp. 135-150, AGU.
607 DOI: 10.1029/AR075p0135.
- 608 Johnson, K. S., et al. (2007), Developing standards for dissolved iron in seawater, *Eos*
609 *Trans. AGU*, 88(11), 131–132, doi:10.1029/2007EO110003.
- 610 Klinck, J. M., and M. S. Dinniman, 2010. Exchange across the shelf break at high
611 southern latitudes, *Ocean Sci.*, 6(2), 513-524. Doi:10.5194/os-6-513-2010.
- 612 Kohut, J., E. Hunter, and B. Huber. 2013. Small-scale variability of the cross-shelf flow
613 over the outer shelf of the Ross Sea, *J. Geophys. Res. Oceans*, 118, 1863–1876,
614 doi:10.1002/jgrc.20090.
- 615 Kohut, J.T., Kustka, A.B., Hiscock, M., Lam, P., Measures, C.I., Milligan, Al., White, A.,
616 Auro, M.E., Carvalho, F., Hatta, M., Jones, B., Ohnemus, D.C., and Swarts, J.M.
617 Mesoscale variability of the summer bloom over the Northern Ross Sea Shelf: A
618 Tale of two Banks. *Journal of Marine Systems* (this issue).
- 619 Kustka, A., Jones, B.M., Hatta, M., Field, M. P., and A. J. Milligan, 2015. The influence
620 of iron and siderophores on eukaryotic phytoplankton growth rates and
621 community composition in the Ross Sea, *Marine Chemistry*. 173. 195-207.
622 doi:10.1016/j.marchem.2014.12.002.
- 623 Lam, P.J., Bishop, J.K.B., 2008. The continental margin is a key source of iron to the
624 HNLC North Pacific Ocean. *Geophysical Research Letters* 35, L07608.
625 doi:10.1029/2008GL033294.

626 Lam, P.J., Bishop, J.K.B., Henning, C.C., Marcus, M.A., Waychunas, G.A., Fung, I.Y.,
627 2006. Wintertime phytoplankton bloom in the subarctic Pacific supported by
628 continental margin iron. *Global Biogeochemical Cycles* 20 (1),
629 doi:10.1029/2005GB002557.

630 Marinov, I., A. Gnanadesikan, J.R., Toggweiler, and J. L. Sarmiento, 2005. The Southern
631 Ocean biogeochemical divide, *Nature*, 441, 964-967, doi:10.1038/natur04883.

632 Marsay, C.M., P.N. Sedwick, M.S. Dinniman, P.M. Barrett, S.L., Mack, and D.J.
633 McGillicuddy Jr. (2014), Estimating the benthic efflux of dissolved iron on the Ross
634 Sea continental shelf, *Geophys. Res. Lett.*, 41, 7576-7583,
635 doi:10.1002/2014GL061684.

636 Martin, J.H., 1990. Glacial–interglacial CO₂ change: the iron hypothesis. *Paleocea-*
637 *nography* 5 (1), 1–13, 10.1029/PA005i001p00001.

638 Martin, J.H., R.M. Gordon, and S.E. Fitzwater, 1991. The case for iron, *Limnol.*
639 *Oceanography* 36(8), 1793-1802.

640 McGillicuddy, D.J., P.N. Sedwick, M.S. Dinniman, K.R. Arrigo, T.S. Bibby, B.J.W.
641 Greenan, E.E Hofmann, J.M. Klinck, W.O. Smith Jr., S.L. Mack, C.M. Marsay,
642 B.M. Sohst and G.L. van Dijken, 2015. Iron supply and demand in an Antarctic
643 shelf ecosystem. *Geophys. Res. Lett.* 42, 8088-8097,
644 doi:10.1002/2015GL065727.

645 Measures, C.I., J. Yang, and J.A. Resing, J., 1995. Determination of iron in seawater by
646 flow injection analysis using in-line preconcentration and spectrophotometric
647 detection, *Mar. Chem.*, **50**, 3-12.

648 Measures, C.I., Vink, S., 2001. Dissolved Fe in the upper waters of the Pacific sector of
649 the Southern Ocean. *Deep-Sea Res. II* 48, 3913–3941, doi:10.1016/S0967-
650 0645(01)00074-1.

651 Measures, C. I., W. M. Landing, M. T. Brown, and C. S. Buck (2008a) A commercially
652 available rosette system for trace metal clean sampling, *Limnol. Oceanogr.*
653 *Methods* 6:384-394. doi: 10.4319/lom.2008.6.384.

654 Measures, C. I., W. M. Landing, M. T. Brown, and C. S. Buck (2008b), High-resolution
655 Al and Fe data from the Atlantic Ocean CLIVAR-CO2 Repeat Hydrography
656 A16N transect: Extensive linkages between atmospheric dust and upper ocean
657 geochemistry, *Global Biogeochem. Cycles*, 22, GB1005,
658 doi:10.1029/2007GB003042.

659 Measures, C.I., M. Hatta, and M.M. Grand. 2012. Bioactive trace metal distributions and
660 biogeochemical controls in the Southern Ocean. *Oceanography* 25(3):122–133,
661 [http:// dx.doi.org/10.5670/oceanog.2012.85](http://dx.doi.org/10.5670/oceanog.2012.85).

662 Measures, C.I., Brown, M.T., Selph, K.E., Apprill, A., Zhou, M., Hatta, M., Hiscock,
663 W.T. 2013. The Influence of Shelf Processes in Delivering Dissolved Iron to the
664 HNLC waters of the Drake Passage, Antarctica, *Deep-Sea Res. II.* 90. 77-88, doi:
665 10.1016/j.dsr2.2012.11.004.

666 Milne, A., W.Landing, M.Bizimis, P. Morton, 2010. Determination of Mn, Fe, Co, Ni,
667 Cu, Zn, Cd and Pb in seawater using high resolution magnetic sector inductively
668 coupled mass spectrometry (HR-ICP-MS). *Analytica Chimica Acta* 665, 200-207.
669 doi:10.1016/j.aca.2010.03.027.

670 Ohnemus, D.C., Auro, M.E., Sherrell, R.M., Lagerstrom, M., Morton, P.L., Twining,
671 B.S., Rauschenberg, S., Lam, P.J., 2014. Laboratory intercomparison of marine
672 particulate digestions including Piranha: a novel chemical method for dissolution
673 of polyethersulfone filters. *Limnology and Oceanography-Methods* 12, 530-547.
674 10.4319/lom.2014.12.530.

675 Ohnemus, D.C., Lam, P.J., 2015. Cycling of lithogenic marine particles in the US
676 GEOTRACES North Atlantic transect. *Deep Sea Research Part II: Topical*
677 *Studies in Oceanography* 116, 283-302, DOI:10.1016/j.dsr2.2014.11.019.

678 Orsi, A. H., and C.L. Wiederwohl. 2009. A recount of Ross Sea waters. *Deep-Sea Res. II.*
679 56. 778-795. doi:10.1016/j.dsr2.2008.10.033.

680 Peloquin, J.A., Smith Jr., W.O., 2007. Phytoplankton blooms in the Ross Sea, Antarctica:
681 interannual variability in magnitude, temporal patterns, and composition. *Journal*
682 *of Geophysical Research* 112, C08013. doi:10.1029/2006JC003816.

683 Raiswell, R., Canfield, D.E., Berner, R.A., 1994. A comparison of iron extraction
684 methods for the determination of degree of pyritisation and the recognition of
685 iron-limited pyrite formation. *Chemical Geology* 111 (1-4), 101-110.

686 Reddy, T. E., and K. R. Arrigo, 2006. Constraints on the extent of the Ross Sea
687 phytoplankton bloom, *J. Geophys. Res.*, 111, C07005,
688 doi:10.1029/2005JC003339.

689 Resing, J. and C.I. Measures. 1994. Fluorimetric determination of Al in seawater by FIA
690 with in-line preconcentration, *Anal. Chem.*, 66,4105-4111.

691 Resing, J. A. and M. J. Mottl. 1992. Determination of Manganese in seawater using flow
692 injection analysis with on-line preconcentration and spectrophotometric,
693 *Analytical Chemistry*, **64**, 2682-2687.

694 Robertson, R., Beckmann, A., H. Hellmer. 2003. M_2 tidal dynamics in the Ross Sea.
695 *Antarctic Science* 15. 41-46. doi:10.1017/S0954102003001044.

696 Schlitzer, R., Ocean Data View, <http://odv.awi.de>, 2015.

697 Sedwick P. N., G. DiTullio, and D.Mackey, 1996. Dissolved iron and manganese in
698 surface waters of the Ross Sea, austral summer 1995-1996, *Antarctic journal of*
699 *the United States* / v.31 no.2. 1996, pp.128-130.

700 Sedwick, P. N., and G.R. DiTullio, 1997. Regulation of algal blooms in Antarctic shelf
701 waters by the release of iron from melting sea ice, *Geophys. Res. Lett.*, 24, 2515-
702 2518, 10.1029/97GL02596.

703 Sedwick, P.N., G.R. DiTullio, D.J. Mackey. 2000. Iron and manganese in the Ross Sea,
704 Antarctica: Seasonal iron limitation in Antarctic shelf waters. *Journal of*
705 *geophysical research*, 105. C5. 11321-11336, doi:10.1029/2000JC000256.

706 Sedwick, P. N., C.M. Marsay, B.M. Sohst, A.M. Aguilar-Islas, M.C. Lohan, M.C. Long,
707 K.R. Arrigo, R.B. Dunbar, M.A. Saito, W.O. Smith, G.R. DiTullio, 2011. Early
708 season depletion of dissolved iron in the Ross Sea polynya: Implications for iron
709 dynamics on the Antarctic continental shelf, *J. Geophys. Res.*, 116, C12019,
710 doi:10.1029/2010JC006553.

711 Smith Jr., W.O. and J.C. Comiso, 2008. Influence of sea ice on primary production in the
712 Southern Ocean: a satellite perspective. *Journal of Geophysical Research* 113,
713 C05S93. doi:10.1029/2007JC004251.

714 Smith W.O., Jr. and L.I. Gordon, 1997. Hyperproductivity of the Ross Sea (Antarctica)
715 polynya during austral spring, *Geophys. Res. Lett.*, 24, 233-236, DOI:
716 10.1029/96GL03926.

717 Sunda W.G. and S.A. Huntsman, 1986. Relationships among growth rate, cellular
718 manganese concentrations and manganese transport kinetics in estuarine and
719 oceanic species of the diatom *Thalassiosira*, *J. Phyco.*, 22. 259-270.
720 DOI: 10.1111/j.1529-8817.1986.tb00022.x.

721 Sunda, W.G., Huntsman, S.A., 1995. Iron uptake and growth limitation in oceanic and
722 coastal phytoplankton. *Mar. Chem.* 50, 189–206, doi:10.1016/0304-
723 4203(95)00035-P.

724 Sullivan, C.W., K.R. Arrigo, C.R., McClain, J.C. Comiso, and J. Firestone, 1993.
725 Distributions of phytoplankton blooms in the Southern Ocean, *Science* 262
726 (5141):1832-7.

727 Takahashi T., Sutherland, S. C., Wanninkhof, R., Sweeney, C., Feely, R.A., Chipman, D.
728 W., Hales, B., Friederich, G., Chavez, F., Sabine, C., Watson, A., Bakker, D. C.
729 E., Schuster, U., Metzl, N., Yoshikawa-Inoue, H., Ishii, M., Midorikawa, T.,
730 Nojiri, Y., Körtzinger, A., Steinhoff, T., Hoppema, M., Olafsson, J., Arnarson, T.

731 S., Tilbrook, B., Johannessen, T., Olsen, A., Bellerby, R., Wong, C. S., Delille, B.
732 D., Bates, N. R., and H.J.W. de Baar, 2009. Climatological mean and decadal
733 change in surface ocean pCO₂, and net sea–air CO₂ flux over the global oceans,
734 Deep Sea Research Part I: 56, Issue 11, 2075-2076, DOI:
735 10.1016/j.dsr2.2008.12.009.

736 Whitworth III, T., and A.H. Orsi. 2006. Antarctic Bottom Water production and export
737 by tides in the Ross Sea. *Geophysical Res Lett.* 33. L12609.
738 doi:10.1029/2006GL026357.

739 Whitworth, T., A. H. Orsi, S.-J. Kim, W.D. J. Nowlin, and R.A. Locarnini. 2013. Water
740 masses and mixing near the Antarctic Slope Front, *Ocean, Ice and Antract. Res.*
741 *Ser.*, 75, 1-29, DOI: 10.1029/AR075p0001.

742

743 **Figures and Tables**

744 **Figure 1.** Map of sampling stations in the Ross Sea during the 2011 SEAFARERS cruise
745 and a sampling station (Station 100) during the subsequent CLIVAR S4P cruise. The
746 sampling stations are shown with blue circles, adjacent to the station's numbers. The red
747 box encompasses the stations that are a section across Drygalsky Basin (DB), Mawson
748 Bank (MB), Joides Basin (JB), Pennell Bank (PB), and Glomar Challenger Basin (GBC).
749 The insert (top left) shows a composite satellite image of Chl-*a* from MODIS during this
750 expedition (blue is lower values and red is higher values of Chl-*a* fluorescence).

751 **Figure 2.** Potential temperature and salinity data from all stations occupied, with selected
752 stations shown in color in order to identify the typical water masses found. Offshore
753 station (Station 14, red circles), one station at the western side of Pennell Bank (Station
754 16, green squares), the inner shelf with MCDW water (Station 2, blue cross), and inner
755 shelf (Station 3, black circles) with less pronounced MCDW features. Station 48 (purple
756 circles) is located above Pennell Bank. Abbreviations: AASW = Antarctic Surface
757 Water; CDW = Circumpolar Deep Water; MCDW = Modified Circumpolar Deep Water;
758 HSSW = High Salinity Shelf Water.

759 **Figure 3.** Distributions of water properties in the section above Pennell and Mawson
760 banks (stations shown in Figure 1) as a function of longitude. (a) Temperature ($^{\circ}\text{C}$), (b)
761 Salinity (psu), (c) Neutral Density (kg/m^3), (d) Fluorescence (volts), (e) Silicate (μM),
762 and (f) Phosphate (μM). **Averaged values are shown at the stations (16/24/41 and 7/61)**
763 **that were occupied repeatedly.**

764 **Figure 4.** Distributions of trace elements in the section above Pennell and Mawson
765 banks (stations shown in Figure 1) as a function of longitude. (a) Leachable particulate Fe
766 (pFe, nM), (b) Total pFe (nM), (c) Percent of leachable pFe (%), (d) dissolved Al (dAl,
767 nM), (e) dissolved Mn (dMn, nM), and (f) dissolved Fe (dFe, nM). **Averaged values are**
768 **shown at the stations (16/24/41 and 7/61) that were occupied repeatedly.**

769 **Figure 5.** Vertical depth (m) profiles of various parameters from the repeated stations on
770 the western side of Pennell Bank (Stations 24, 24, and 41) and the offshore station
771 (Station 14). (a) temperature ($^{\circ}\text{C}$), (b) dissolved Fe (dFe, nM), (c) dissolved Mn (dMn,

772 nM), (d) salinity (psu), (e) leachable pFe (nM), (f) total pFe (nM). The depth of the core
773 of the MCDW is shown by the star (*) symbol on the profile and its colour is the same as
774 the station's data colour.

775 **Figure 6.** The vertical depth (m) profiles of parameters from the repeated stations at the
776 top of Pennell Bank (Stations 7, 61, and 48). (a) temperature (°C), (b) dissolved Fe (dFe,
777 nM), (c) dissolved Mn (dMn, nM), (d) fluorescence (volts), (e) leachable pFe (nM), (f)
778 **Brunt-Vaisala Frequency (cycl/h).**

779 **Figure 7.** Property-property plots (salinity vs. various properties and dFe vs. dMn) of the
780 MCDW and CDW (neutral density = 28.0~28.27 kg/m³), at the repeated stations along
781 the western side of Pennell Bank (Stations 16, 24, 41; all MCDW stations), the inshore
782 station (Station 3) that is less modified with MCDW water, and offshore station (Station
783 14, CDW station). Salinity is plotted as a function of: (a) potential temperature, (b)
784 silicate (µM), (c) dFe (nM), (d) dMn (nM), and (e) dAl (nM). Finally, (f) dFe is plotted
785 as a function of dMn from the MCDW stations.

786 **Table 1.** Station locations (refer to Fig 1), and Mixed Layer Depth (MLD, db), maximum
787 fluorescence depth (Max. FL depth, m), and the depth of 1% PAR. The MLD and 1%
788 PAR depth from the hydrographic rosette are indicated with a “*” in their column
789 headers.

790 **Table 2.** Station water mass characteristics. Shown are station locations, averaged dFe
791 and dMn (nM), fluorescence signals (FL, volts), and the density ranges for each water
792 mass. A question mark in the Water Mass column indicates that the identity of the water
793 masses is not clear from the available data. Abbreviations: AASW = Antarctic Surface
794 Water; CDW = Circumpolar Deep Water; MCDW = Modified Circumpolar Deep Water;
795 **MSW = Modified Shelf Water; SW= Shelf Water;** MB = Mawson Bank; PB = Pennell
796 Bank, DB = Drygalsky Basin; JB = Joides Basin; GBC = Glomar Challenger Basin. **The**
797 **values with the (*) symbol are the average values within the defined density range.**

798 **Table 3.** The leachable and total pFe concentrations (L-pFe and T-pFe, respectively, nM)
799 in the water masses at stations occupied in the Ross Sea, with the station regions
800 indicated. Abbreviations: AASW = Antarctic Surface Water; CDW = Circumpolar Deep

801 Water; MCDW = Modified Circumpolar Deep Water; MSW = Modified Shelf Water;
802 SW= Shelf Water; MB = Mawson Bank; PB = Pennell Bank, DB = Drygalsky Basin; JB
803 = Joides Basin; GBC = Glomar Challenger Basin.

804

805 **Table 1.** Station locations (refer to Fig 1), and Mixed Layer Depth (MLD, db), maximum fluorescence depth (Max. FL depth, m), and
 806 the depth of 1% PAR. The MLD and 1% PAR depth from the hydrographic rosette are indicated with a “*” in their column headers.

807

Location	Station #	Longitude	Latitude	MLDs [db]	Max. fluorescence depth [m]	MLDs*	1% PAR depth [m]*
Offshore	14	178.00	-74.50	40.00	10-46	28	43
Offshore	30	178.75	-74.20	19.00	20-50	22	24
DB	55	173.17	-73.08	74.00	0-74	55	50
above MB	70	174.00	-73.35	49.00	60-90	43	65
JB	35	174.83	-73.58	33.00	24-48	33	36
JB	100	175.83	-73.88	40.00	20-70	No data	No data
JB	16	176.67	-74.13	32.00	62-104	31	82
JB	24	176.66	-74.14	25.00	23-58	14	58
JB	41	176.67	-74.13	38.00	21-40	37	66
above PB	7	178.00	-74.50	30.00	22-47	41	22
above PB	61	178.00	-74.50	40.00	10-46	51	23
above PB	48	178.75	-74.20	40.00	49-61	19	61
GBC	28	179.50	-74.87	44.00	10-44	40	28
Inner shelf	2	174.00	-75.19	43.00	33-60	32	No data
Inner shelf	3	178.52	-76.16	44.00	10-45	40	54
Inner shelf	21	177.00	-75.75	39.00	10-30	44	24

808

809

810 **Table 2.** Station water mass characteristics. Shown are station locations, averaged dFe and dMn (nM), fluorescence signals (FL,
811 volts), and the density ranges for each water mass. A question mark in the Water Mass column indicates that the identity of the water
812 masses is not clear from the available data. Abbreviations: AASW = Antarctic Surface Water; CDW = Circumpolar Deep Water;
813 MCDW = Modified Circumpolar Deep Water; **MSW = Modified Shelf Water; SW= Shelf Water;** MB = Mawson Bank; PB = Pennell
814 Bank, DB = Drygalsky Basin; JB = Joides Basin; GBC = Glomar Challenger Basin. **The values with the (*) symbol are the average**
815 **values within the defined density range.**

Water mass	Region	Station #	dFe (nM)	dMn (nM)	fluorescence (volts)	neutral density range
AASW within mixed layer	Offshore	14	0.16	0.24	0.39	
	DB	55	0.08*	0.45*	0.39*	
	above MB	70	0.16*	0.35*	0.37*	
	JB	35	0.18	0.08	0.92	
	JB	100	0.20	0.11	0.57	
	JB	16	0.17	0.1	0.31	
	JB	24	0.19	0.17	0.81	
	JB	41	0.11	0.36	0.4	
	above PB	48	0.13*	0.17*	0.48*	
	above PB	7	0.15*	0.05*	1.73*	
	above PB	61	0.25	<0.05	1.66	
	GCB	28	0.16	0.05	1.42	
	Inner shelf	2	0.13*	0.35*	0.4*	
	Inner shelf	3	0.19*	0.13*	0.51*	

	Inner shelf	21	0.18*	0.09*	1.46*	
CDW	Offshore	14	0.36*	0.11*		28.00-28.27
MCDW	DB	55	0.26*	0.37*		28.02-28.12
	above MB	70	0.28*	0.37*		28.03-28.08
	JB	35	0.26*	0.54*		28.03-28.08
	JB	100	0.26*	0.42*		28.03-28.08
	JB	16	0.30*	0.34*		28.03-28.20
	JB	24	0.22*	0.49*		28.05-28.19
	JB	41	0.24*	0.46*		28.03-28.14
	above PB	61	0.28*	0.74*		28.00-28.03
	above PB	48	0.24*	0.53*		27.99
	above PB	7	0.23*	0.37*		28.00-28.03
MCDW	GCB	28	0.22*	0.39*		28.00-28.15
MCDW	Inner Shelf	2	0.26*	0.58*		28.04-28.10
	Inner Shelf	3	0.21*	0.73*		28.00-28.06
	Inner Shelf	21	0.31*	0.51*		28.01-28.06
MSW&SW	DB	55	0.25-0.53	0.44-0.65		>28.27, HSSW
	JB	35	0.38-0.40	0.47-0.50		>28.27, MSW
	JB	100	0.25-0.56	0.34-0.79		>28.27, HSSW
	JB	16	0.28-0.35	0.32-0.44		>28.27, MSW
	JB	24	0.33-0.64	0.40-0.89		>28.27, HSSW
	JB	41	0.25-0.36	0.43-0.78		>28.27, MSW
	GBC	28	0.28-0.47	0.44-0.88		>28.27, MSW
	Inner shelf	2	0.35-0.76	0.78-1.44		>28.27, HSSW
	Inner shelf	3	0.22-0.73	0.78-2.17		>28.27, LSSW

	Inner Shelf	21	0.30-0.37	0.42-1.12		>28.27, MSW
--	-------------	----	-----------	-----------	--	-------------

816

817

818 **Table 3.** Leachable and total pFe concentrations (L-pFe and T-pFe, respectively, nM) in the water masses at stations occupied in the
819 Ross Sea, with the station regions indicated. Abbreviations: AASW = Antarctic Surface Water; CDW = Circumpolar Deep Water;
820 MCDW = Modified Circumpolar Deep Water; **MSW = Modified Shelf Water; SW= Shelf Water**; MB = Mawson Bank; PB = Pennell
821 Bank, DB = Drygalsky Basin; JB = Joides Basin; GBC = Glomar Challenger Basin.

Water mass	Region	Station #	L-pFe (nM)	T-pFe (nM)
AASW	offshore	14	0.079	0.169
	DB	55	0.073	0.166
	above MB	70	0.054	0.095
	JB	35	0.045	0.053
	JB	24	0.042	0.047
	above PB	7	0.12	0.313
	GBC	28	0.101	0.387
CDW	offshore	14	0.075	0.213
MCDW	DB	55	0.93	2.75
	above NB	70	0.99	3.35
	JB	24	1.01	3.07
	above PB	7	0.72	2.76
MSW & SW	DB	55	2.68	8.03
	JB	35	2.28	8.76
	JB	24	2.15	6.84

Figure 1
[Click here to download high resolution image](#)

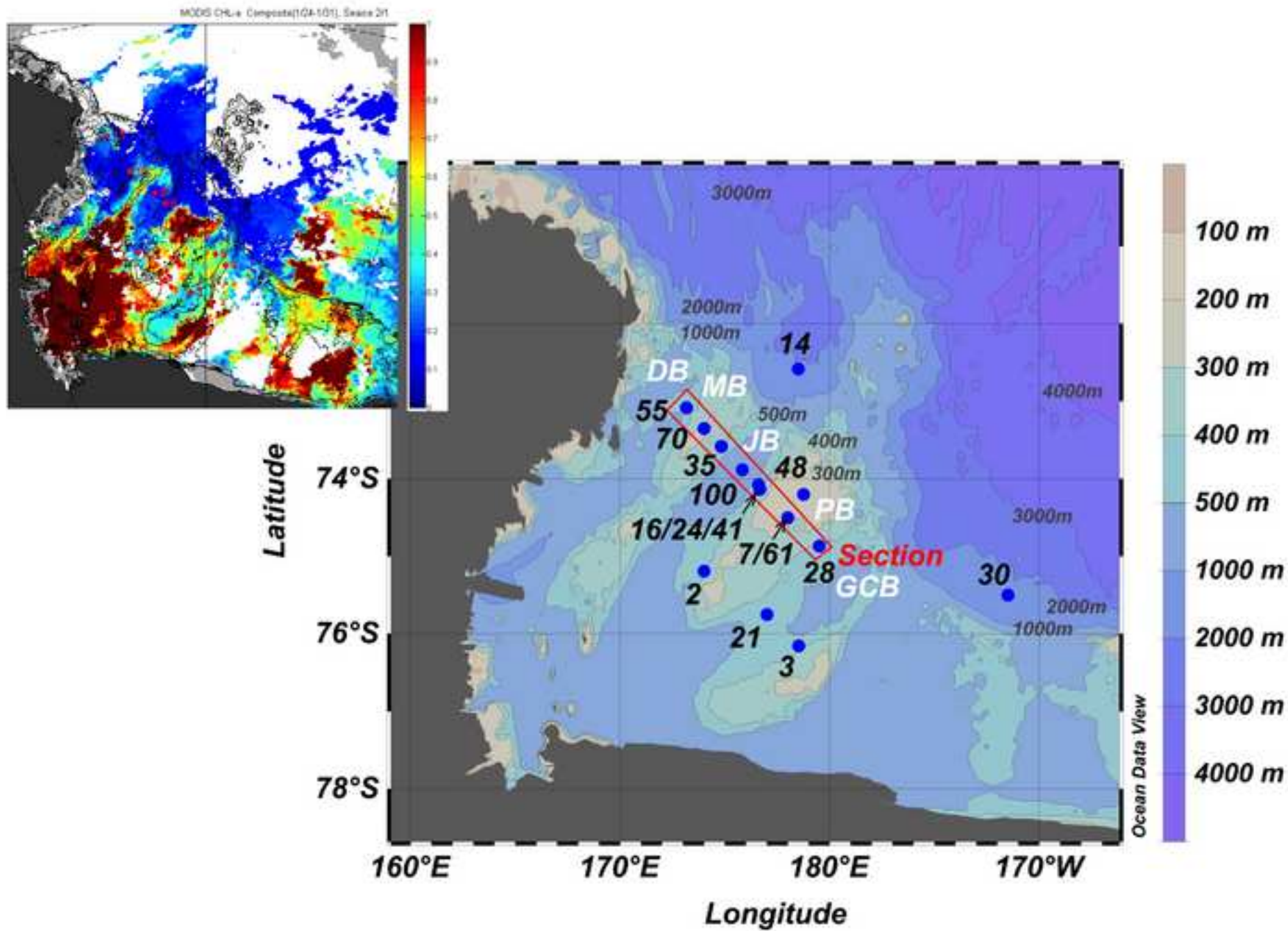


Figure 2 revised
[Click here to download high resolution image](#)

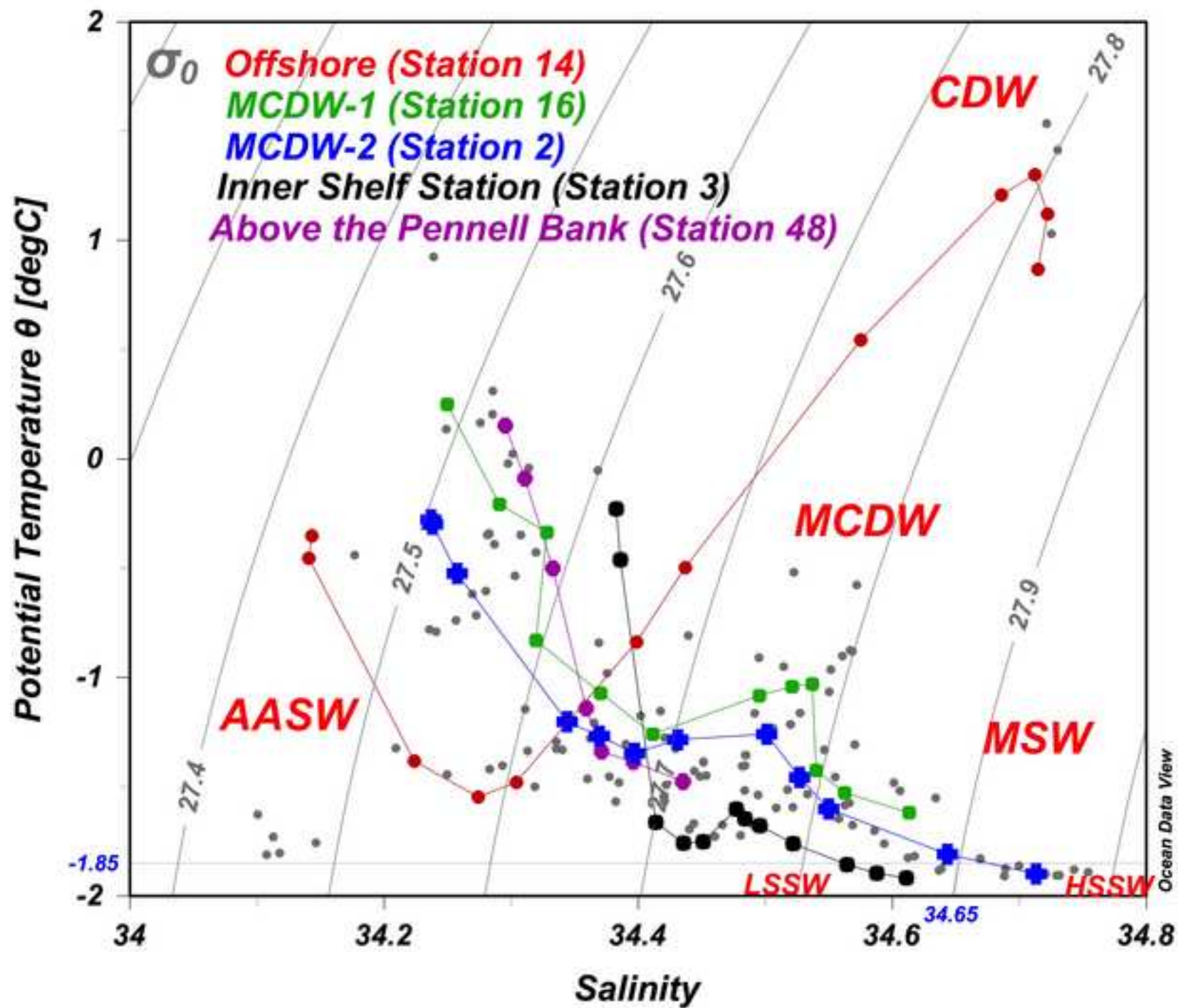


Figure 3 revised
[Click here to download high resolution image](#)

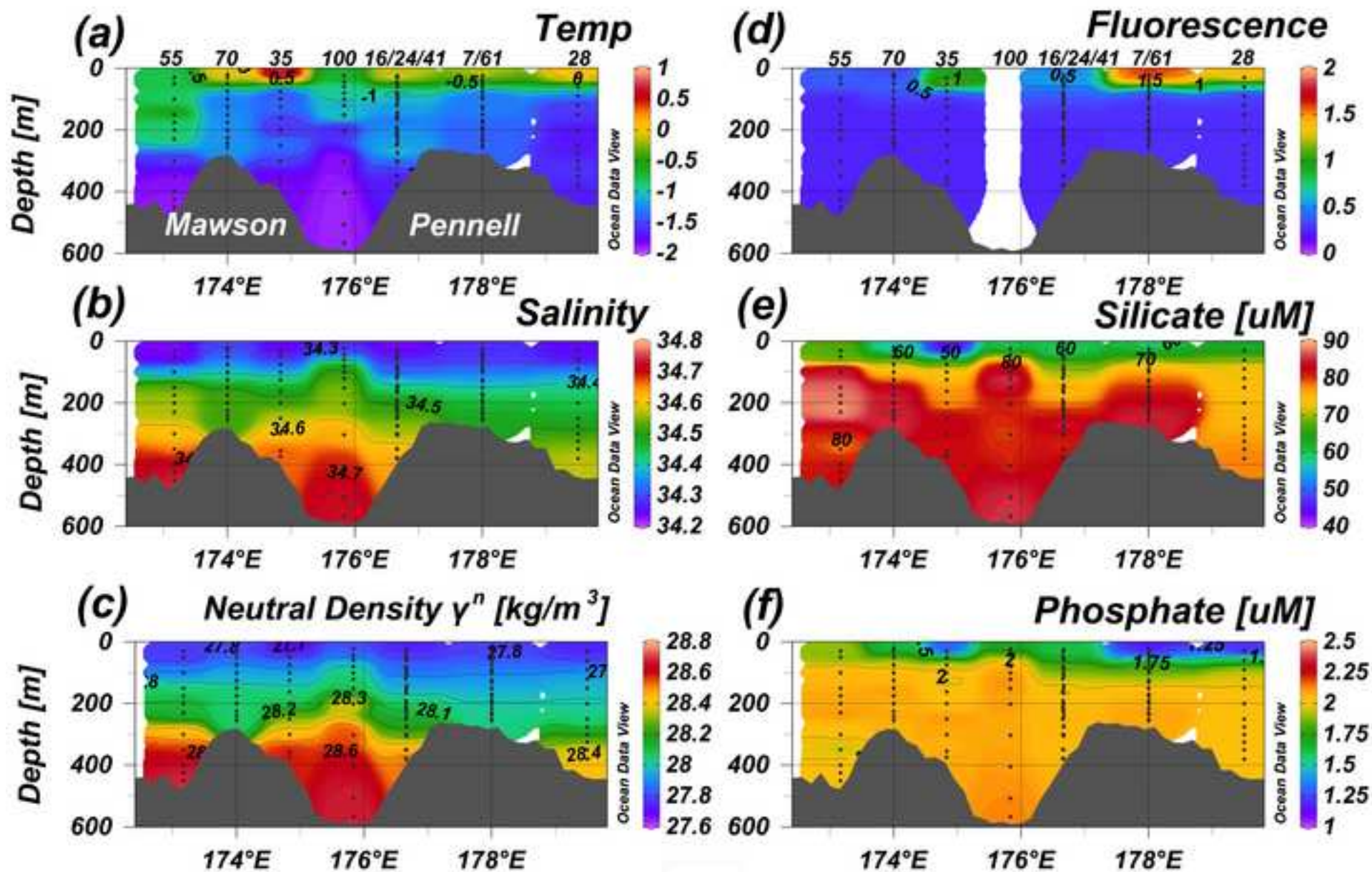


Figure 4 revised
[Click here to download high resolution image](#)

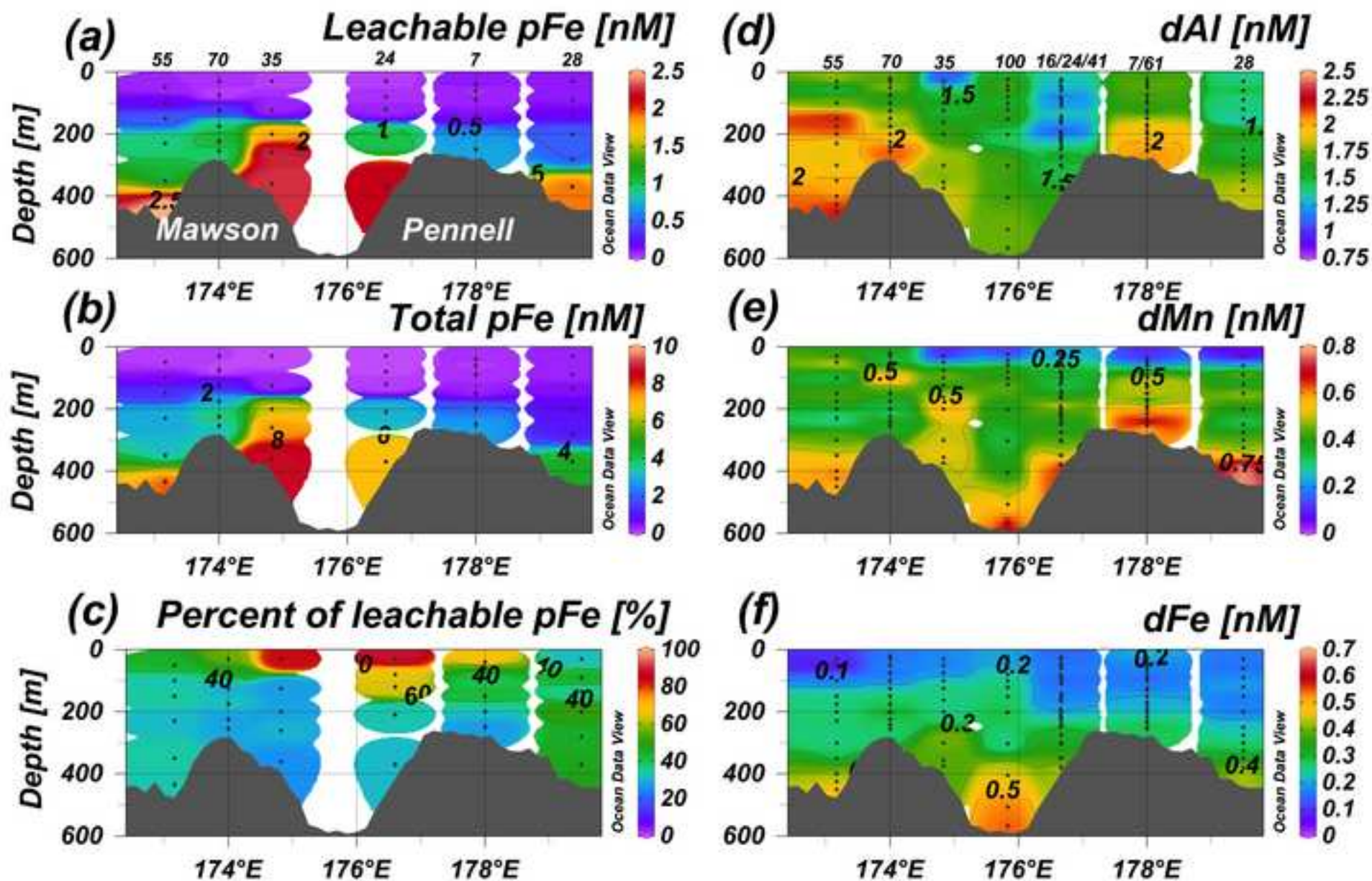


Figure 5 revised
[Click here to download high resolution image](#)

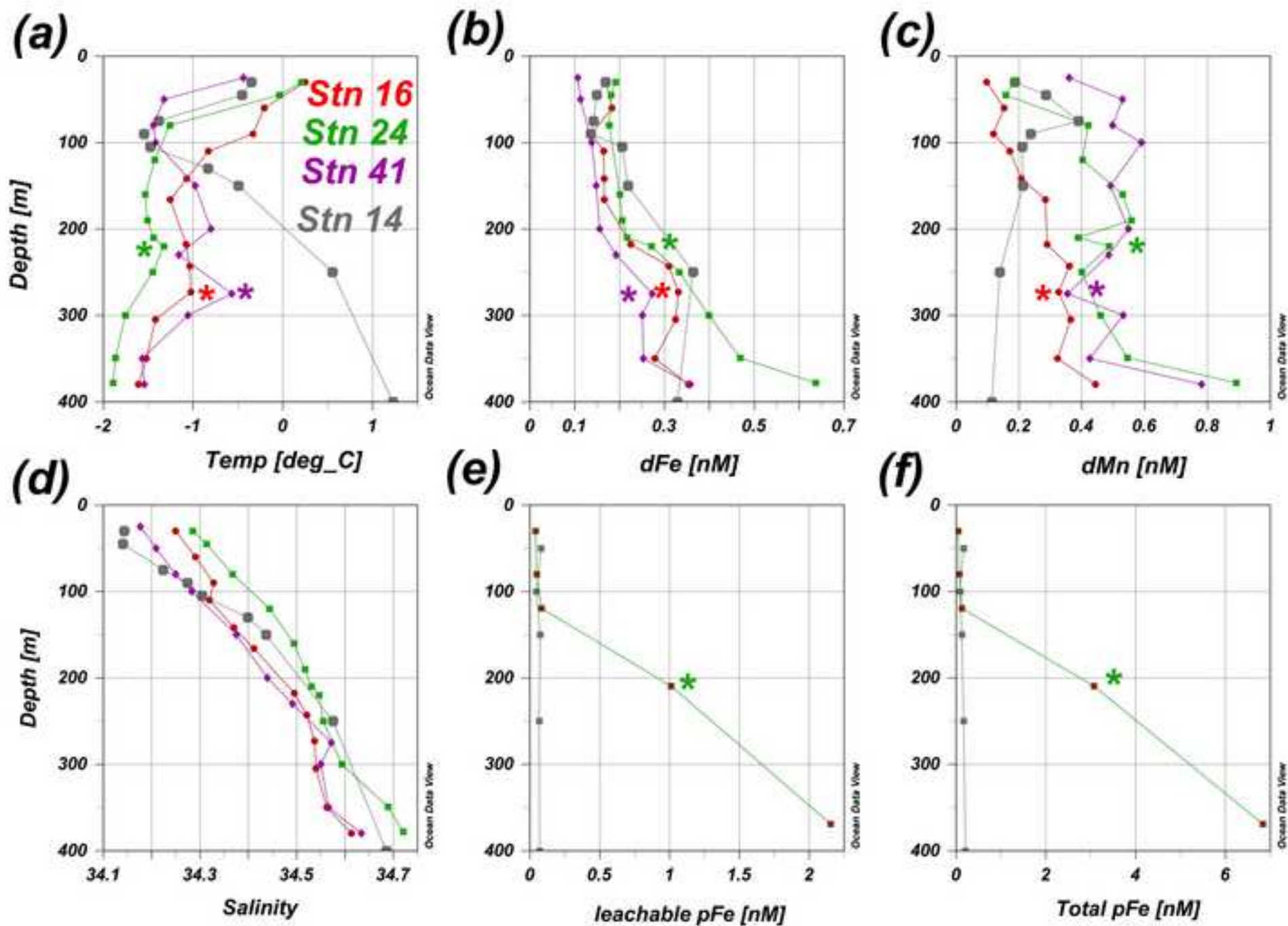


Figure 6 revised
[Click here to download high resolution image](#)

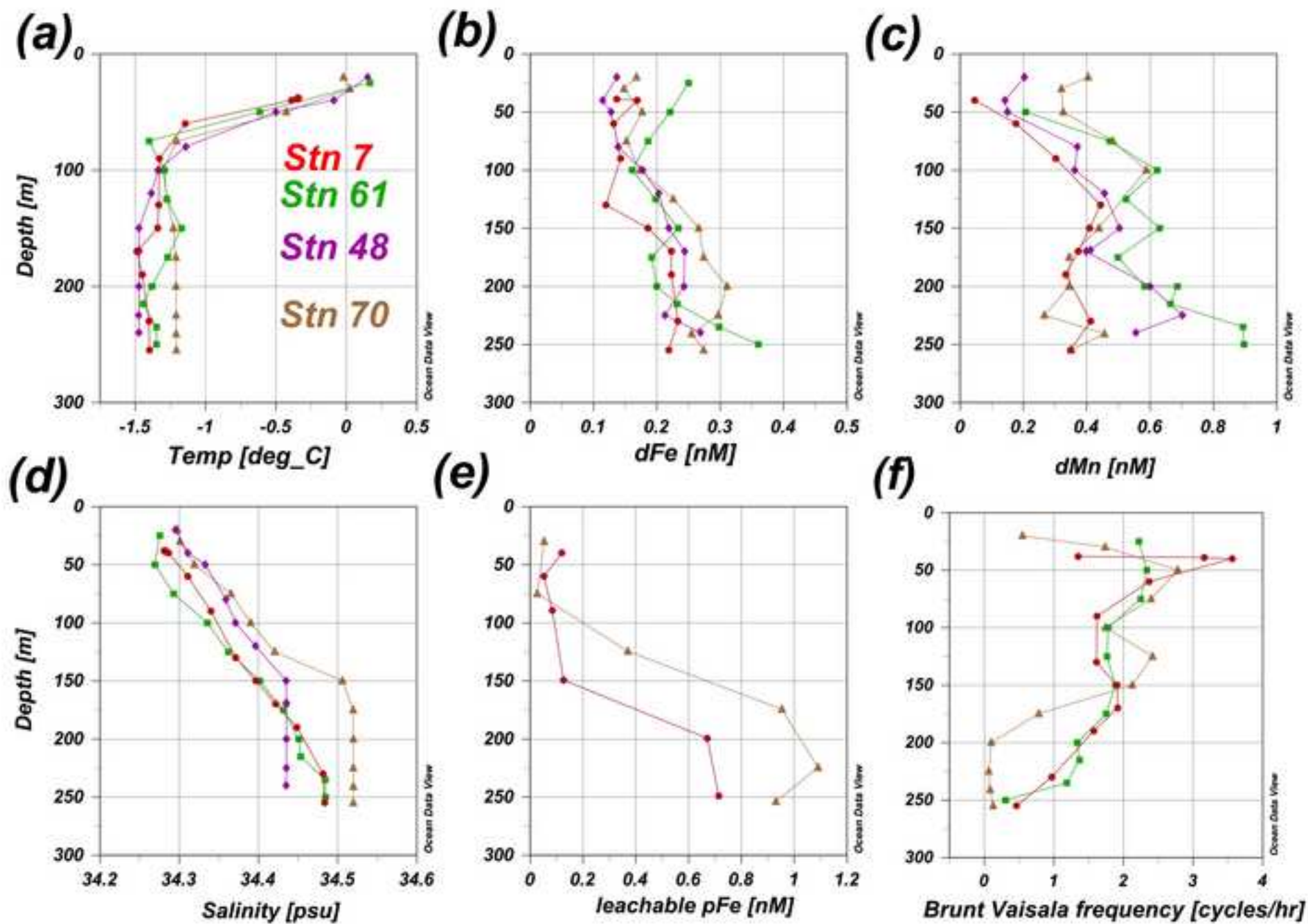


Figure 7 revised
[Click here to download high resolution image](#)

